ELSEVIER

Polymer 40 (1999) 1525–1536

polymer

Effect of peel rate and temperature on delamination toughness of PC–SAN microlayers

T. Ebeling, A. Hiltner*, E. Baer

Department of Macromolecular Science and Center for Applied Polymer Research, Cleveland, OH 44106-7202, USA

Received 24 February 1998; accepted 12 May 1998

Abstract

The effect of peel rate and temperature on peel toughness and delamination failure mode of coextruded microlayer sheet consisting of alternating layers of polycarbonate (PC) and poly(styrene-co-acrylonitrile) (SAN) was studied with the T-peel test. Microlayers with thin ($<1.5\ \mu$m) SAN layers always failed by interfacial delamination and consequently the interfacial toughness was independent of rate and temperature. In microlayers with thicker SAN layers, the crack alternately propagated through crazes in the SAN and along a PC–SAN interface at intermediate peel rates. The length of the crack-tip zone, the number of crazes and the amount of craze fracture increased with increasing peel rate; the peel toughness increased accordingly. Extending the tests through eight decades in peel rate revealed a transition from craze-dominated cohesive fracture at intermediate rates to predominately interfacial fracture at either very high or very low peel rates. Transitional peel behaviour resulted from the rate sensitivity of yielding and crazing in SAN as determined from tensile tests of bulk polymer.

Keywords: Polycarbonate; Poly(styrene-co-acrylonitrile); Microlayers

1. Introduction

Polycarbonate and poly(styrene-co-acrylonitrile) (SAN) can be coextruded as a continuous microlayered sheet with hundreds of alternating layers. Synergistic interaction of the two components, as exemplified by the increased toughness and impact resistance when the layer thickness is reduced to the micron scale, is only possible because adhesion between the components is good enough to ensure stress transfer under conditions of high deformation. To determine the PC–SAN adhesive strength, previous studies employed the straightforward T-peel method to delaminate PC/SAN microlayers. A strong effect of layer thickness on delamination toughness was found [1–3]. With SAN layers thinner than 1.5 μm and PC layers thicker than 1.7 μm the crack propagated along a single interface; damage in front of the crack tip was minimal and the peel toughness of 90 J/m^2 corresponded to the interfacial toughness. With thicker SAN layers, crazes formed in front of the crack tip; the crack alternately propagated through the crazes and along an interface. The extent of crazing and amount of cohesive craze fracture increased as the SAN thickness increased. Correspondingly, the peel toughness increased as high as 650 J/m^2 for thick SAN layers. With both interfacial and craze delamination, the crack could move from layer to layer if the PC layers were thin enough. Tearing of the thin PC layers increased the peel toughness.

It is anticipated that transitions in deformation behaviour, such as those observed in the delamination of PC/SAN microlayers, will be affected by testing rate and temperature. Most adhesion studies that considered effects of rate and temperature utilized rubbery polymeric adhesives. The failure mode often changed from cohesive to interfacial as the temperature was reduced or the peel rate was increased [4,5]. Typically a pronounced drop in peel strength accompanied the transition. This behaviour was explained by identifying the cohesive fracture with the liquid-like state and the adhesive fracture with the rubber-like state of the adhesive [6]. According to this interpretation, a sufficiently soft adhesive under sufficiently large peel forces cavitates internally before adhesive failure occurs. Growth of the cavities distributes the peel forces over relatively large bonded areas and is responsible for the unexpectedly large peel forces; bursting of the cavities accounts for the filamentous cohesive fracture surfaces. Because the effective elastic modulus of the rubber, and hence the stress necessary to bring about cavitation, increases with increasing rate of deformation, the adhesive bond fails at higher rates before

* Corresponding author.

0032-3861/98/$ - see front matter
PII: S0032-3861(98)00386-3

Table 1
Microlayer composition and layer thicknesses

No. layers	Volume ratio (PC/SAN)	Estimated layer thicknesses PC (μm)	SAN (μm)
49	65/35	34	18
194	88/12	9.1	1.5
927	85/15	2.5	0.5

cavitation occurs. This accounts for the transition to interfacial failure and low peel strength at high rates of peel or low temperatures. Crazing is also a cavitational process, and similar concepts might apply to transitional phenomena in the delamination of glassy polymers.

Previous studies of glassy adhesives focused primarily on the effect of joint thickness [7,8]. These efforts were motivated by the strong thickness dependence of peel toughness, which is analogous to the effect of layer thickness in PC/SAN microlayers. It is a general phenomenon in peel of glassy polymer joints that crazing ahead of the crack tip inhibits fracture by distributing the load surrounding the crack, thus causing crack growth to consume large amounts of energy. Thickness effects arise when the size scale of the craze is comparable to the layer thickness [9,10]. Reduction of the joint thickness confines the craze zone and reduces the peel toughness [11].

The rate and temperature dependence of bulk crazing is well known. The general trend is towards fewer, shorter crazes as strain rate decreases [12]. This and other features, particularly a continuous increase in craze thickness with decreasing rate, are understandable in terms of an increasing contribution of chain disentanglement [13,14]. The present study extends our investigation of peel toughness of PC–SAN microlayers to the effect of rate and temperature. The measurements are correlated with observations on SAN crazing in microlayers and in the bulk.

2. Experimental

Coextruded microlayer sheets were supplied by The Dow Chemical Company [1]. Sheets about 1 mm in thickness consisted of alternating layers of polycarbonate (PC) and poly(styrene-co-acrylonitrile) (SAN). The number of layers and the extruder feed ratios were varied to produce microlayers with different compositions and layer thicknesses—see Table 1. Microlayers are defined by the average layer thicknesses, which were calculated from the measured bulk thickness, the total number of layers and the feed ratio.

The PC was Merlon M-40 (Mobay) with a molecular weight of 28 000–30 000 reported by the manufacturer. The SAN was Tyril 1000B (previously Tyril 867B) (Dow) with a molecular weight of 193 000 and a polydispersity of 1.9 as determined by GPC relative to polystyrene standards with the appropriate correction [15]. The 25% acrylonitrile content reported by the manufacturer was confirmed by FTIR.

Delamination was carried out with the T-peel test (ASTM D 1876). Specimens 15–25 mm wide were notched by pushing a fresh razor blade into the midplane of the sheet. The notch was examined with an optical microscope to ensure that the crack started along a single layer. Specimens were peeled at room temperature and various rates ranging from 0.002 to 220 mm/min as the load was recorded. Additional specimens were peeled at 2000 and 20 000 mm/min without recording the load. In order to eliminate specimen-to-specimen scatter, individual specimens were peeled at various rates beginning at 200 mm/min; after the crack propagated about 10–15 mm, the specimen was unloaded and reloaded at successively slower peel rates of 20, 2, 0.2, 0.02 and 0.002 mm/min.

Other specimens were peeled at 2.0 mm/min and various temperatures ranging from -95°C to 85°C. Individual specimens were peeled at various temperatures to eliminate specimen-to-specimen scatter. After the temperature equilibrated for 15 min, the specimen was loaded at 2.0 mm/min until the crack propagated about 10–15 mm. The specimen was unloaded and the temperature re-equilibrated. Specimens were either initially loaded at a low temperature and sequentially heated, or loaded at a high temperature and sequentially cooled. The heating/cooling pattern did not affect the results.

Some tests were interrupted and the crack tip region was sectioned perpendicular to the plane of the crack with a low-speed diamond saw (Isomet, Buehler Ltd). The sections were polished on a metallurgical wheel with wet sandpaper and alumina oxide aqueous suspensions and photographed in a transmission optical microscope. Sections of the fracture surfaces were coated with 90 Å of gold for examination in a JEOL JSM 940A scanning electron microscope. Uncoated sections of the fracture surface were analysed with the Nicolet 800 FTIR spectrometer in the ATR mode with a germanium 60/60 crystal to determine the surface composition.

Tensile testing of compression-moulded SAN specimens was carried out at various strain rates in an Instron 1123 testing machine. The fracture stress was measured from the peak of the stress–strain curves obtained with ASTM D638 specimens. With the same specimen geometry, the tensile modulus was measured at strains less than 0.5% using a strain gauge.

A 1 mm radius semicircular notch was machined midway along one edge of a rectangular SAN specimen, 120 mm $\times$ 20 mm. The notched bars were pulled at crosshead speeds ranging from 0.001 to 10 mm/min with an initial grip separation of 100 mm. The growth of crazes in the triaxial stress state at the notch root was monitored by a video camera equipped with a travelling optical microscope. The published solution for the elastic field in front of a semicircular edge notch was used to analyse the craze zone [16]. In some cases, specimens were loaded to specific

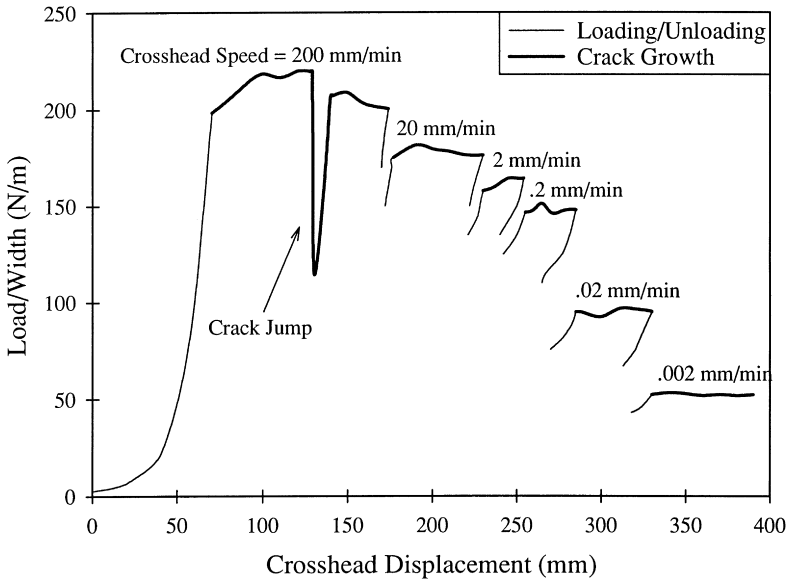

Fig. 1. Peel curve from a single specimen of PC/SAN (34 μm/18 μm) peeled at a series of decreasing rates from 200 to 0.002 mm/min. The thick lines indicate periods of loading during which the crack propagated, the thin lines indicate periods of loading prior to crack growth and periods of unloading.

positions on the stress–displacement curve and removed from the Instron for further characterization of the craze zone. For the optical microscope, a small section containing the craze zone was trimmed and microtomed to the desired depth using an RMC ultramicrotome (MT6000-XL).

3. Results

3.1. Effect of peel rate

The peel curve in Fig. 1 is from a single specimen of PC/SAN (34 μm/18 μm) peeled at a series of decreasing rates. The thick lines indicate periods of loading during which the crack propagated; the thin lines indicate periods of loading prior to crack growth and periods of unloading. Continuous crack propagation at a relatively constant load P_c enabled the delamination toughness, $G = 2P_c/W$, to be calculated for a specimen of width W. At 200 mm/min an occasional crack jump, accompanied by a load drop, interrupted the stable crack growth; in this case, the delamination toughness was measured from the regions of stable crack growth. Crack propagation was continuous at all rates lower than 200 mm/min. At the higher rates, delamination toughness of individual specimens decreased slightly with decreasing peel rate. The peel toughness decreased more dramatically at slower rates, by about 40% for each order of magnitude in peel rate.

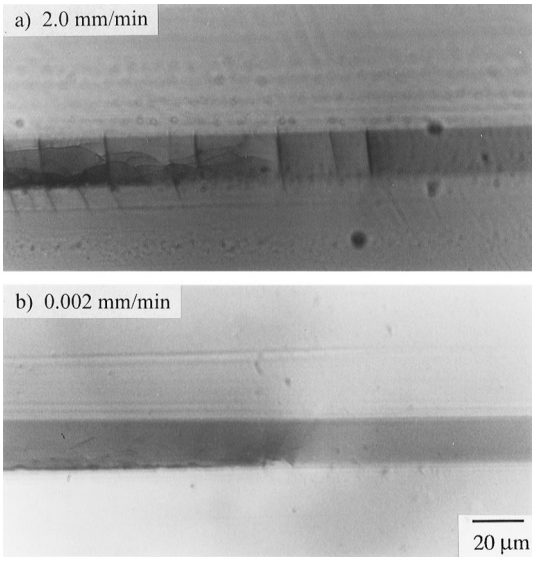

Fig. 2. Optical micrographs of the crack tip of PC/SAN (34 μm/18 μm) at two peel rates.

A reduction in the size of the crack tip craze zone and a decrease in the amount of cohesive fracture accounted for the drop in delamination toughness with decreasing peel rate. The micrographs in Fig. 2 compare the crack tip of PC/SAN (34 μm/18 μm) at two peel rates. At 2.0 mm/min the craze zone in the SAN layer extended about 150 μm ahead of the crack tip (Fig. 2a). Crazes grew from the crack tip or out of other crazes, then curved over the closest interface. Crazing was not uniformly distributed through the SAN layer, but was concentrated in one half of the layer. The crack propagated alternately through the crazes and along the closest interface. Additional vertical crazes spanning the SAN layer perpendicular to the crack growth direction might have been promoted by residual stresses in the SAN [17]. This specimen, with considerable crazing and cohesive fracture of the SAN, had a peel toughness of 320 J/m^2. A similar craze zone preceded the crack tip in regions of stable crack growth at a peel rate of 200 mm/min and the crack path was mixed mode with both cohesive craze fracture and interfacial fracture.

Table 2
Modulus and yield stress of SAN

Strain rate (%/min)	Modulus (GPa)	Yield stress[b] (MPa)
10.0000	3.5	98
1.0000	3.4	94
0.1000	3.3	90
0.0100	3.2	86
0.0010	3.1[a]	82
0.0001	3.0[a]	77
0.00001	2.9[a]	72

[a] Extrapolated from data at higher rates.
[b] Extrapolated from high pressure data[18].

Table 3
Calculated craze zone size

Peel rate (mm/min)	Measured G (J/m^2)	r_p (μm)
0.002	100	6.3
0.02	180	11.0
0.2	290	18.0
2.0	390	25.0
20.0	380	24.0
200.0	430	27.0

Compared to the 2.0 mm/min peel rate, the craze zone was slightly longer, 180 μm compared to 150 μm, and there were a few more crazes. This accounted for the slightly higher peel toughness of 400 J/m^2.

At the slowest peel rate, 0.002 mm/min, the craze zone was much shorter, about 20 μm, and consisted of only a few crazes. The micrograph in Fig. 2b shows that the crack propagated primarily along the interface. The crack occasionally propagated through crazes in the SAN layer, but only through short crazes close to the interface. With decreased amounts of crazing and craze fracture, the peel toughness of 100 J/m^2 approached the interfacial toughness.

The visual evidence of crazing clearly indicated that the deformation zone was a major factor in delamination of PC/SAN microlayers. To obtain a relationship between craze zone size and delamination toughness, a plastic zone analysis was used. In previous studies that modelled the increase in fracture toughness with adhesive layer thickness [10], Irwin's equation for the size of the plastic zone (r_p) in plane stress showed the best correlation with toughness

$$r_p = \frac{EG}{2\pi\sigma_y^2} \quad (1)$$

The Young's modulus (E) was measured at four strain rates— see Table 2. The tensile yield stress (σ_y) at one strain rate (0.1%/min) was obtained by extrapolating the pressure-dependent yield stress of SAN to 1 atm[18]; the yield stress at other strain rates was calculated with the rate-dependency of the polystyrene yield stress[19]. The factor in rate used to correlate σ_y and E from tensile measurements with G from peel measurements did not significantly affect the results; the factor of 200 was arbitrarily chosen. Using the measured delamination toughness, r_p was calculated for the microlayer with 18 μm thick SAN layers. The results for r_p in Table 3 correlate with the thickness of the craze zone. Like the craze zone, r_p increases gradually with peel rate to a limiting value at higher rates that is approximately equal to the thickness of the SAN layer. It follows that the SAN layer thickness determines the maximum size of the plastic zone, and therefore controls the maximum delamination toughness achievable at higher peel rates.

3.2. Peel fractography

Infrared analysis of peel fracture surfaces revealed that one surface had only SAN (SAN surface) and the other had PC and some SAN (PC surface). The PC surfaces of PC/SAN (34 μm/18 μm) peeled at 2.0 and 0.002 mm/min are compared in Fig. 3. The PC surface in Fig. 3a shows two textures separated by a white boundary: a smooth featureless texture and a rough porous texture. Previously, infrared analysis revealed the smooth, featureless region to be the surface of a PC layer and the rough porous region to be SAN [1]. The porous texture of the SAN regions was characteristic of craze fracture. The islands of craze fracture were up to 300 μm wide and several hundred microns long. About 65% of the surface contained craze fracture features. Tilting the sample in the SEM revealed the bright lines separating

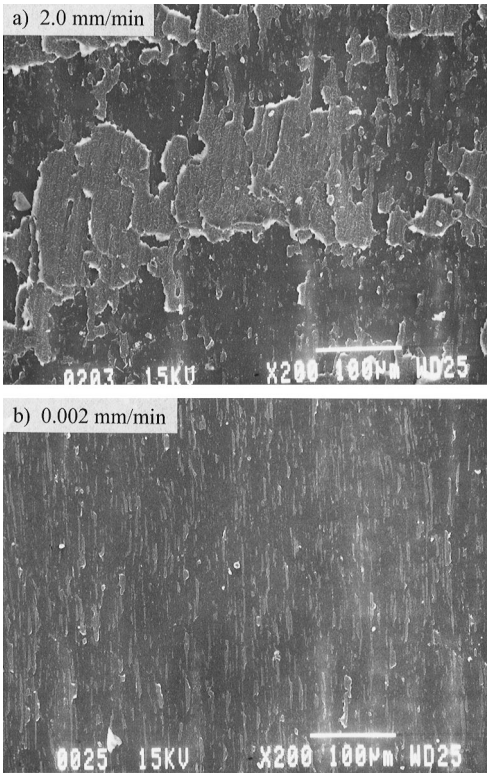

Fig. 3. Scanning electron micrographs of the PC fracture surface at two peel rates. The crack propagated from left to right.

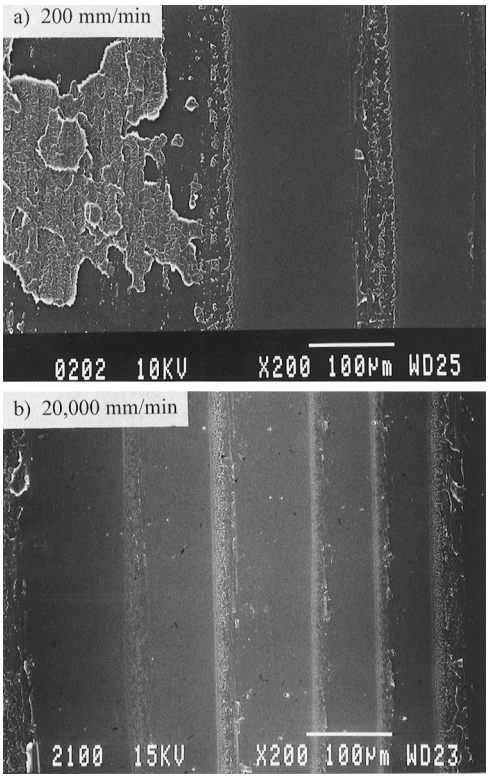

Fig. 4. Scanning electron micrographs of the PC fracture surface at higher peel rates. The crack propagated from left to right.

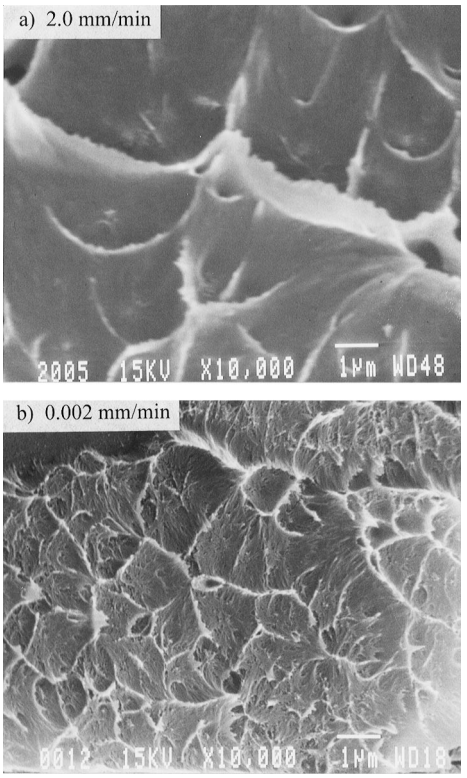

Fig. 5. Higher magnification scanning electron micrographs of craze fracture on the peel fracture surfaces in Fig. 3.

the regions of craze and interfacial fracture to be level difference lines about 10 μm in height, about half the SAN layer thickness. The SAN surface, not shown, had matching regions of porous craze fracture and smooth interfacial failure [1]. Light scattering from the rough areas of craze fracture caused both the PC and the SAN fracture surfaces to be visually opaque for a peel rate of 2.0 mm/min.

At a peel rate of 0.002 mm/min the PC fracture surface was transparent and the SAN surface was slightly translucent. The micrograph in Fig. 3b shows the smooth PC surface with very small islands of crazed SAN. The length of the SAN craze islands, about 5 μm, correlated with the length of the crazes in the damage zone. Only about 20% of the fracture surface was covered with SAN craze islands. Decreases in the size of the crack tip craze zone and the amount of craze fracture accounted for the decrease in delamination toughness.

Fracture surfaces of PC/SAN (34 μm/18 μm) from a 200 mm/min peel rate in Fig. 4a exhibited a texture very similar to that of the 2.0 mm/min peel (Fig. 3a) in regions of stable crack growth, and in addition smooth areas of interfacial fracture that corresponded to the crack jumps. Often, just before the crack jump there was an increase in the amount of interfacial fracture. Apparently as more of the crack found its way to the interface the resistance to crack growth decreased. When enough of the crack front moved to the interface the elastic energy stored in the beam arms exceeded the energy required for interfacial crack growth and a crack jump occurred. Once the excess stored energy was spent the crack arrested and subsequently grew in the normal continuous mode. This behaviour suggested that a transition from craze to interfacial failure might occur at high peel rates. The possibility was tested by peeling specimens at 2000 and 20 000 mm/min. Although the peel toughness could not be measured accurately at these rates, the 20 000 mm/min fracture surface in Fig. 4b showed predominantly large, featureless regions of interfacial crack propagation periodically separated by thin crack arrest lines that contained craze features. Peeling at 2000 mm/min produced the same features. Extending the tests through eight decades in peel rate revealed a transition from the craze-dominated fracture at intermediate rates to predominantly interfacial fracture at either very high or very low peel rate.

When craze fracture occurred, higher magnification revealed a rate dependency of craze morphology. Fig. 5a from the surface peeled at 2.0 mm/min shows a porous texture consisting of fractured fibrils and membrane-like connections between fibrils. Fig. 5b, at the same magnification, shows much smaller pores and many more fractured fibrils on the surface peeled at 0.002 mm/min. Although craze fibrils recoil and change dimensions upon fracture, the micrographs clearly show that the diameter of the fibrils decreased and the fibril density increased as the peel rate decreased.

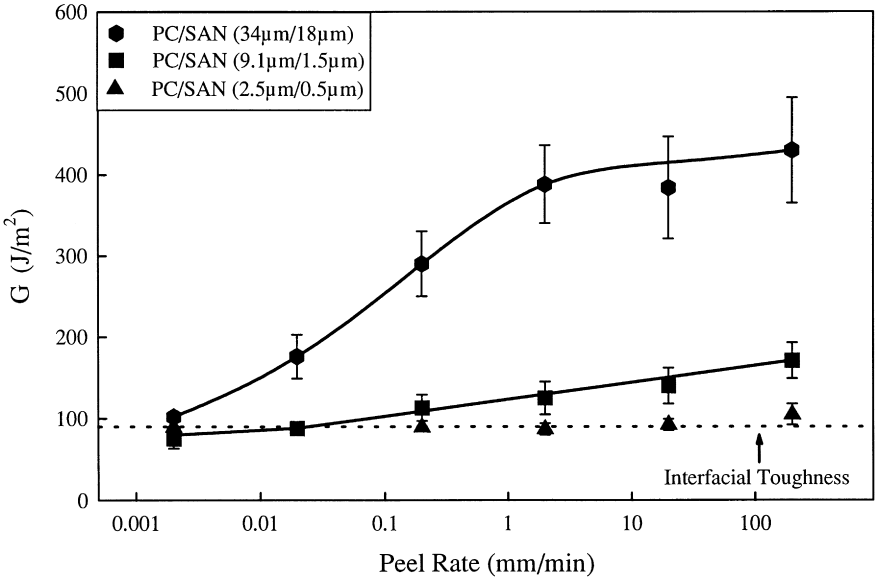

Fig. 6. The effect of peel rate on delamination toughness of microlayers with different SAN layer thicknesses.

3.3. Effect of SAN layer thickness on delamination

The effect of peel rate on delamination toughness of microlayers with different layer thicknesses is illustrated in Fig. 6. The data confirmed the strong dependence on SAN layer thickness reported previously [1]. However, the effect was remarkable only at higher peel rates (the previous study used a peel rate of 2.0 mm/min). As the peel rate decreased, the delamination toughness of thicker SAN layers decreased to approach the toughness of thin SAN layers. The decrease in toughness of thicker SAN layers paralleled the change from predominately craze delamination to predominately interfacial delamination. In contrast to thick SAN layers, interfacial delamination always dominated the failure of thin SAN layers and the delamination toughness did not depend on peel rate. At low peel rates all the microlayers, regardless of SAN layer thickness, failed by predominately interfacial delamination with about the same toughness of 90 J/m^2.

Fig. 7(a–f) are micrographs of PC fracture surfaces from the three microlayers in Fig. 5 peeled at 200 mm/min and 0.002 mm/min. In the stable crack growth regions of the microlayer with 18 μm thick SAN layers peeled at a rate of 200 mm/min, about 65% of the fracture surface contained craze fracture features (Fig. 7a). At 0.002 mm/min the peel surface still had some craze fracture features (Fig. 7b); however, it showed much more interfacial fracture than the 200 mm/min peel surface. Also, the length of the craze islands had decreased to about 5 μm, which corresponded to the length of the crazes in front of the crack tip.

The fracture surface in Fig. 7c shows the sample with 1.5 μm thick SAN layers peeled at 200 mm/min. In addition to craze fracture features, the surface exhibited evidence that the crack propagated along both interfaces of the SAN layer. This was inferred from the presence of two interfacial failure textures. Interfacial failure on one side of the SAN layer created the occasional smooth dark areas that identified the surface of underlying PC layer, and failure on the other side of the SAN layer left smooth areas of SAN that did not contain the porous craze texture. Regions of porous craze texture separated the areas of interfacial delamination, which indicated that the crack propagated through SAN crazes as it moved from one interface of the SAN layer to the other [1]. The lower peel toughness compared to the 18 μm thick SAN was due to the smaller size of the craze zone and the lesser amount of craze fracture. As the peel rate decreased, interfacial propagation was confined to one interface of the 1.5 μm SAN layers, and the craze islands on the fracture surface were smaller indicating a shorter craze zone at the notch tip. At a peel rate of 0.002 mm/min, the crack propagated along a single interface and occasionally through a small craze (Fig. 7d).

Fracture surfaces of the microlayer with 0.5 μm thick SAN layers exhibited only features of interfacial fracture, with no evidence of crazing at the crack tip or on the fracture surface regardless of the peel rate. At 200 mm/min, the crack often tore through the SAN layer leaving scraps of SAN on the PC surface (Fig. 7e). The peel strength was slightly higher than the interfacial toughness, 100 J/m^2 compared to 90 J/m^2, due to the contribution of SAN tearing. At a slower peel rate (Fig. 7f), the smooth PC surface was littered with only a few small chunks of SAN and the peel toughness corresponded to the interfacial toughness.

3.4. Effect of temperature

The temperature dependence of the microlayer peel toughness is shown in Fig. 8 for three SAN layer thicknesses. Measurements were made with a peel rate high enough to reveal the effects of layer thickness (2 mm/min).

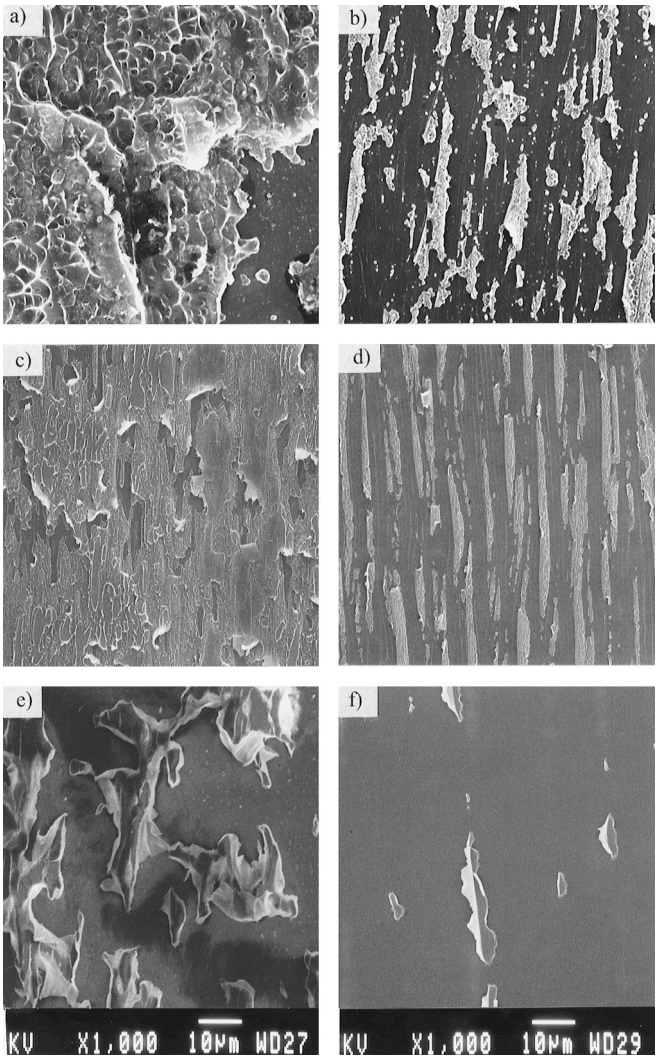

Fig. 7. Scanning electron micrographs of PC fracture surfaces from microlayers peeled at two rates: PC/SAN (34 μm/18 μm) at (a) 200 and (b) 0.002 mm/min; PC/SAN (9.1 μm/1.5 μm) at (c) 200 and (d) 0.002 mm/min; and PC/SAN (2.5 μm/0.5 μm) at (e) 200 and (f) 0.002 mm/min.

Between −55°C and 60°C, the peel toughness decreased gradually with increasing temperature from 470 to 300 J/m^2 for the 18 μm thick SAN layers. As the temperature approached the glass transition temperature of the SAN at 105°C, the peel toughness dropped rapidly, approaching the interfacial toughness. The fracture surfaces reflected the large change in peel toughness with a change from profuse craze fracture at −55°C to interfacial fracture with occasional, small craze islands at 85°C.

The 1.5 μm thick SAN layers exhibited a similar trend characterized by a gradual decrease in the peel toughness from 180 J/m^2 at −55°C to the interfacial toughness of 90 J/m^2 at the highest temperatures. The peel toughness decreased gradually over the entire temperature range. The fracture surfaces exhibited features of both interfacial and craze fracture at all temperatures with smaller craze islands, indicative of a smaller craze zone, as the temperature increased. The peel toughness of the microlayer with 0.5 μm SAN layers was about 90 J/m^2 independent of temperature. Increasing temperature (Fig. 8) had essentially the same effect on the peel toughness of these three microlayers as decreasing rate (Fig. 6). Adjusting the abscissae to obtain superposition produced an equivalence of a 20°C temperature change to a one decade change in peel rate.

3.5. Crazing of bulk SAN

Fig. 9 shows stress versus displacement curves for the semicircular notched tensile tests of SAN at several extension rates. The first damage observed was discontinuous surface crazes that followed curved trajectories. At a slightly higher stress, indicated by the arrows, internal crazes initiated at the notch surface. They grew away from the notch surface following linear trajectories. The tips of the internal notch crazes defined a zone that was initially crescent-shaped and gradually assumed a triangular shape as the stress increased. The specimens eventually fractured through a craze in the centre of the zone. The

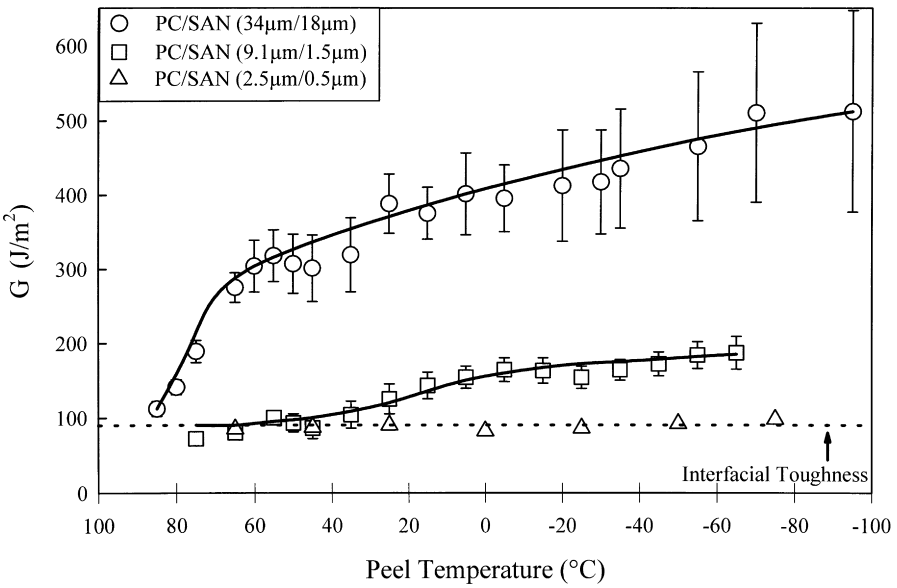

Fig. 8. The effect of peel temperature on delamination toughness of microlayers with different SAN layer thicknesses.

increase in fracture stress with rate resulted in an increase in toughness, defined as the area under the stress–strain curve. Previous studies of PS with blunt notches showed a similar phenomenon [12]. The increase in ultimate tensile toughness with increasing rate paralleled the trend in peel behaviour. The much more pronounced increase in peel toughness was attributed to the mechanics of the test. It has been suggested that stress redistribution due to crazing is much more influential in peel than in uniaxial tension [20,21].

Evidence of yielding was found in specimens deformed at low rates. Under crossed polars, a fractured specimen stretched at 0.01 mm/min showed a small region of residual strain birefringence; the length, about 100 μm, was shorter than the craze zone. At a rate of 0.001 mm/min, the birefringent zone was larger, its length of more than 600 μm exceeded the length of the craze zone. Specimens deformed at 0.1 mm/min or faster exhibited no evidence of residual strain birefringence.

Higher stresses were required for craze initiation and growth as the rate increased. This effect is evident in Fig. 10(a—c) where craze zones are compared at the same stress, 30 MPa, for specimens loaded at 1.0, 0.1 and 0.01 mm/min. At 1.0 mm/min, no internal notch crazes had initiated. At 0.1 mm/min, numerous crazes formed a cresent-shaped zone about 100 μm long. At 0.01 mm/min the zone length increased to 350 μm, although the crazes were less numerous. In general, as the rate decreased, the

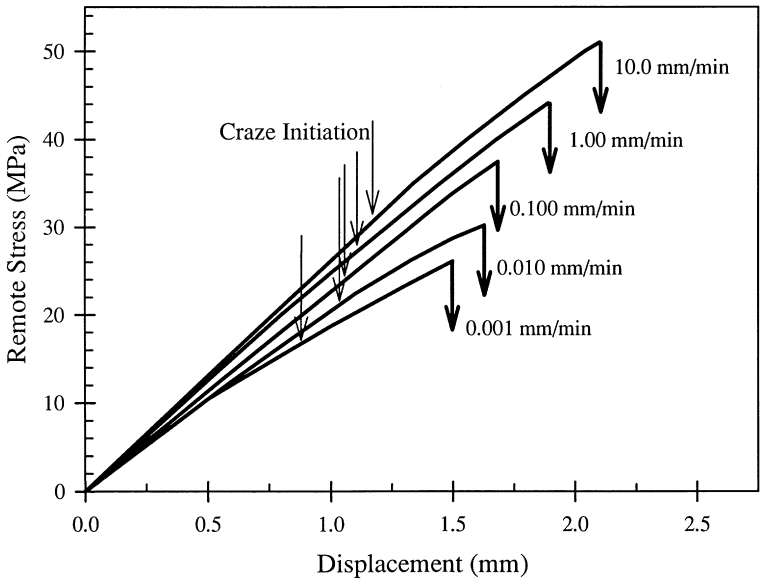

Fig. 9. The effect of extension rate on the stress versus displacement curve of SAN with a semicircular notch.

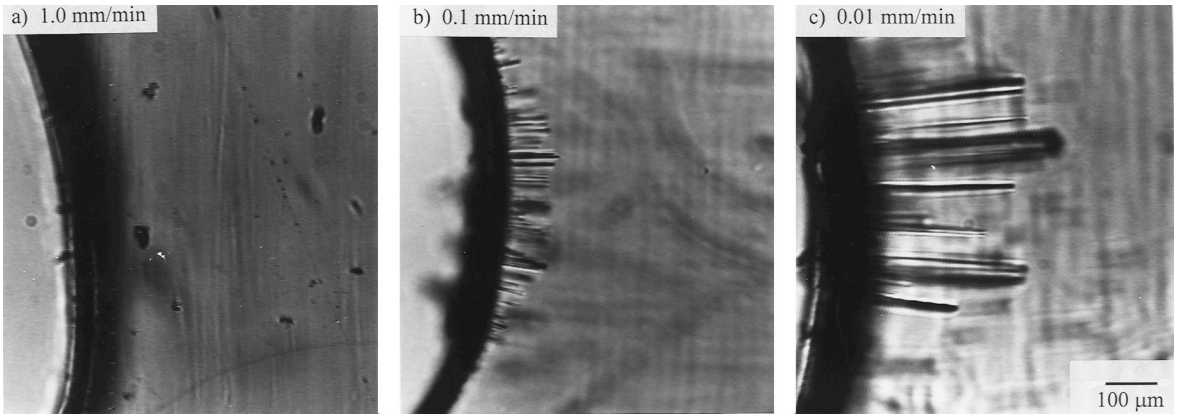

Fig. 10. Optical micrographs of the craze zone in SAN specimens loaded at three extension rates, all at a stress of 30 MPa.

craze zone lengthened and the craze density diminished in accord with previous observations [12].

To illustrate the effect of rate on craze density, specimens were loaded at two strain rates until the longest craze was 300 μm and sectioned through the damage zone about 75 μm from the notch tip. In addition to discontinuous surface crazes, which were visible where they penetrated 10–150 μm inward from both surfaces, the cross-sections in Fig. 11 showed many internal notch crazes. At the higher loading rate, the crazes were much more closely spaced than with the slower loading rate. The number of crazes formed at 10 mm/min was almost twice the number formed at 0.01 mm/min, 75 compared to 42. On the other hand, the average craze width was about the same, 210 μm at the higher rate compared to 190 μm at the slower rate. Thus, the amount of craze surface area almost doubled with three orders of magnitude increase in rate. Higher rate favoured craze initiation over chain disentanglement and craze widening as the mechanism for accommodating strain.

Low magnification SEMs of the fracture surfaces showed the features typical of craze fracture in brittle glassy polymers such as polystyrene and poly(methyl methacrylate). Crack propagation through pre-existing crazes created a smooth region abutting the notch and extending to the banded hackle region (Fig. 12). The length of the pre-existing craze zone at fracture increased with increasing rate. For the specimen deformed at 10 mm/min this region extended about 700 μm from the notch matching the length of the craze zone measured during the test. In contrast, the corresponding region for the specimen pulled at 0.01 mm/min extended about 450 μm ahead of the notch. With the faster extension rate the smooth region reached from edge to edge. Because individual crazes did not extend across the width of the specimen (see Fig. 11), the crack had to propagate through multiple crazes. The white level difference lines marked where the multiple crack paths impinged during final separation. With an extension rate of 0.01 mm/min the smooth region did not reach from edge to edge and there were fewer level difference lines.

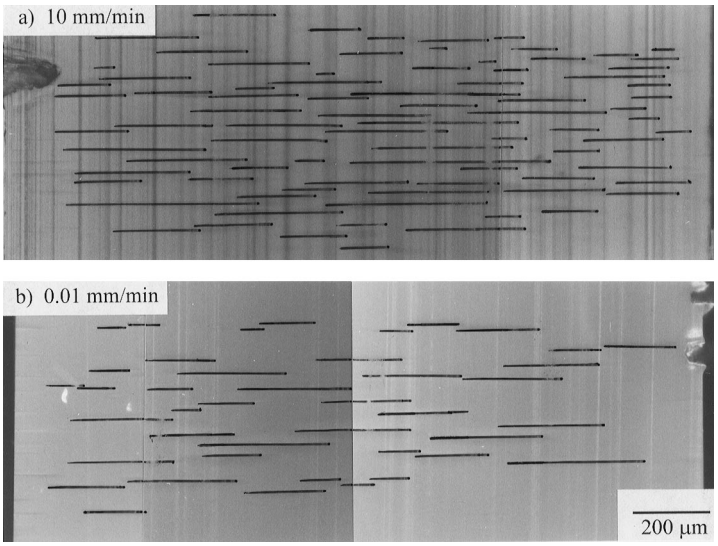

Fig. 11. Cross-sections of the craze zone at two extension rates. The individual crazes are highlighted.

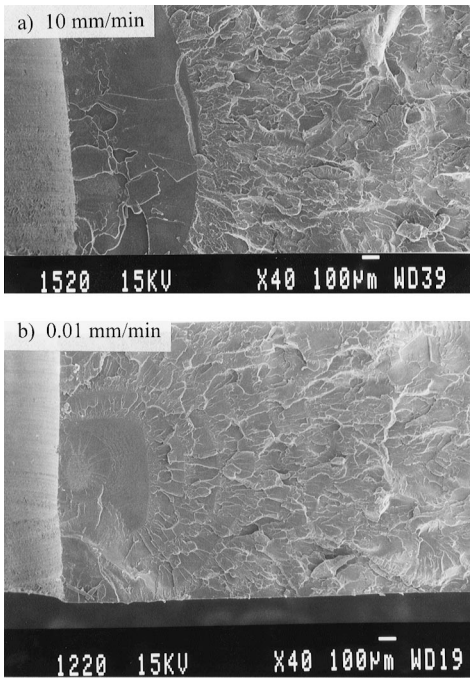

Fig. 12. Scanning electron micrographs of fracture surfaces from semicircular notched SAN specimens at two extension rates. The notch is on the left.

The lessened tendency of the crack to propagate through multiple crazes was consistent with greater separation of crazes.

The hackles in the final region formed when the crack nucleated a set of crazes close to its tip and then propagated along one of these crazes. The hackle texture was continuous at the higher extension rate. At the slower extension rate, the local stress apparently relaxed briefly during rapid propagation and the crack slowed enough for a new set of crazes to form at the crack tip. Repetition of this process caused the crack to propagate by jumps and created the characteristic banding of the hackle pattern.

3.6. Relationship between craze delamination and bulk crazing

The condition for craze growth in SAN was determined from the stress state at the craze tip. The crescent shape defined by the locus of the internal craze tips resembled both the σ_1 and σ_m elastic stress contours, suggesting that a constant stress condition characterized the craze zone boundary. To distinguish between the two possibilities, values of σ_1 and σ_m at the tip of each internal notch craze are plotted in Fig. 13 as a function of the polar angle measured with the origin at the centre of the semicircular notch. The principal stresses σ_1 and σ_2 were obtained as described previously [16] and in the case of plane strain $\sigma_3 = \nu(\sigma_1 + \sigma_2)$. A value of Poisson's ratio $\nu = 0.35$ was used to obtain the mean stress $\sigma_m = (\sigma_1 + \sigma_2 + \sigma_3)/3$. The deviation from the mean in σ_m was less than 5%. On the other hand, the major principal stress σ_1 exhibited a decreasing trend from the edges of the zone to the centre. The excellent correspondence between the craze zone contour and the calculated elastic iso-mean stress contours indicated a critical mean stress condition (σ_{mc}) for the craze growth. Furthermore, the mean stress condition suggested that a cavitation process controlled craze growth. The critical mean stress was obtained for each deformation rate from small craze zones formed at remote stresses not more than 5 MPa above the craze initiation stress. Fig. 14 shows a linear increase in σ_{mc} with exponential loading rate.

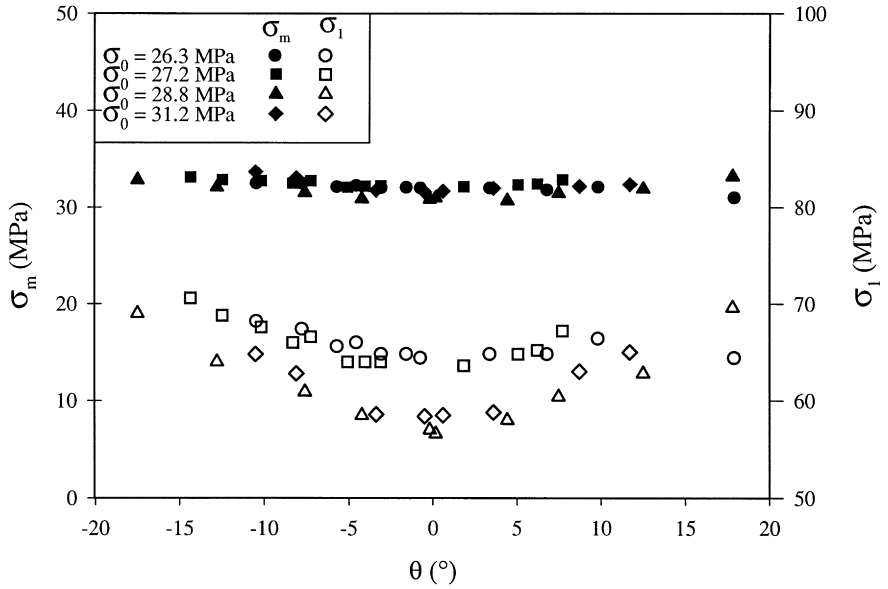

Fig. 13. Values of σ_1 and σ_m at the tip of each internal notch craze at four values of the remote stress (σ_o) plotted as a function of the polar angle measured with the origin at the centre of the semicircular notch.

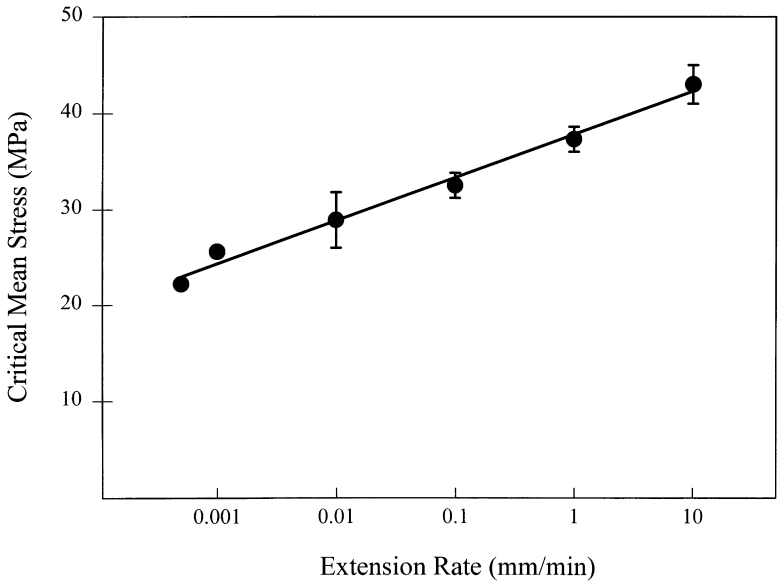

Fig. 14. Dependence of the critical mean stress (σ_{mc}) on extension rate.

As the crazing condition becomes more severe with increasing rate, a transition from crazing to interfacial delamination might be anticipated. This would occur when the craze condition exceeds the rate-independent condition for interfacial failure [2]. To compare the notched tension experiments with the peel tests at equivalent strain rates, a factor of 200 was assumed, i.e. a deformation rate of 0.1 mm/min in notched tension produced the same local strain rate as a deformation rate of 20 mm/min in peel. To correct for the difference in stress state, proportionality was assumed between σ_{mc} and the craze condition in the peel test (G_{craze}), i.e. $G_{craze} = K\sigma_{mc}$. A value of $K = 2.44$, taken together with the strain rate factor of 200, gave the craze condition for peel plotted in Fig. 15. Although calculation of K for this situation is beyond the scope of the study, the magnitude of K is consistent with estimates from the stress distribution in the T-peel test [22]. The craze condition lies below the interfacial toughness of 90 J/m^2 at lower peel rates, and therefore the delamination mode should be crazing. A transition to interfacial delamination is predicted at a peel rate of about 150 mm/min where the craze condition crosses the interfacial toughness. This is totally consistent with the experiment. Interfacial crack jumps at 200 mm/min suggest that this peel rate is close to the transition, tests at 2000 and 20 000 mm/min confirm the transition from craze delamination to interfacial failure.

The tensile results also invite correlations with peel at low rates where a gradual decrease in peel toughness parallels a

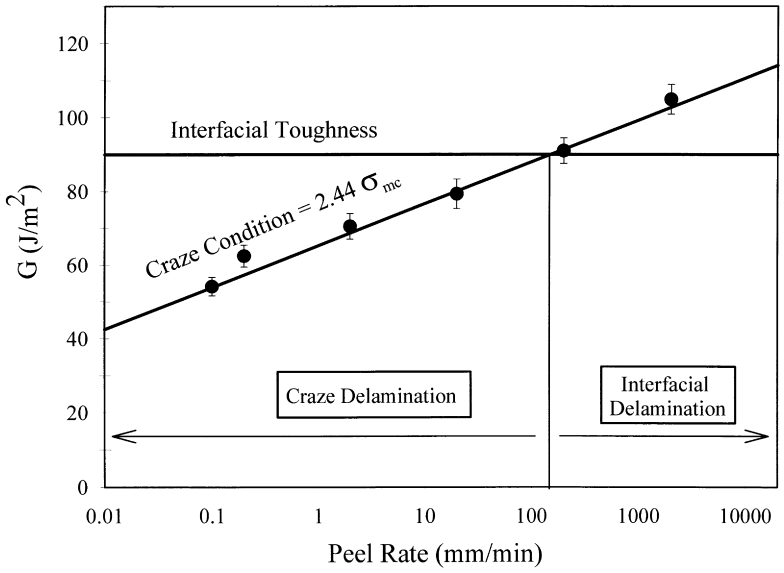

Fig. 15. Comparison of the interfacial toughness with the craze condition (G_{craze}) in the peel test.

change from predominantly craze fracture to predominately interfacial fracture. The decrease in σ_{mc} with decreasing rate would seem to predict an increased propensity for crazing at low rates. However, lower rate (and higher temperature) are conditions that favour craze growth by chain disentanglement over surface drawing; this leads to fewer crazes and ultimately to a transition to yielding. It is known that at ambient temperature and pressure SAN is close to this transition [23,24]. At low rates, yielding blunts the flaws that would be initiation sites for crazes, and delamination proceeds by interfacial failure. The rates where residual birefringence is observed in tensile tests, 0.01 mm/min and especially 0.001 mm/min, are equivalent to peel rates of 2.0 and 0.2 mm/min, which are in the range where reduced crazing and increased interfacial failure account for the gradual drop in delamination toughness.

In summary, the interfacial toughness of PC–SAN microlayers is a measure of the adhesive strength of SAN to PC and appears to be essentially independent of rate and temperature. Because the interfacial toughness is comparable to the crazing condition in the brittle SAN layers, the mode of delamination depends on the competition between interfacial failure and crazing. Changes in the delamination mode (and resulting peel toughness) as a function of external variables such as rate and temperature directly correlate with craze characteristics of the SAN layer. Thus the rate dependence of the SAN craze stress produces a transition from craze to interfacial delamination as the rate increases. The thickness of the SAN layer determines the maximum size of the crack tip craze zone and thus controls the peel toughness of the craze delamination mode. In addition, the appearance of SAN yielding at low rates results in another, more gradual transition from craze to interfacial failure. A parallel change in delamination mode with increasing temperature probably reflects an analogous transition from crazing to yielding, although this was not studied here.

Acknowledgements

This work was generously supported by the Army Research Office, grant DAAL03-92-G-0241 and the National Science Foundation, grant DMR97-05696.

References

[1] Ebeling T, Hiltner A, Baer E. J Appl Polym Sci, in press.
[2] Hiltner A, Ebeling T, Shah A, Mueller C, Baer E. In: Lohse DJ, Russell TP, Sperling LH, editors, Interfacial aspects of multicomponent polymer materials. New York: Plenum, 1997:95–106.
[3] Mueller CD, Nazarenko S, Ebeling T, Schuman TL, Hiltner A, Baer E. Polym Engng Sci 1997;37:355.
[4] Bright WM. In: Clark J, Rutzler JE, Savage RL, editors, Adhesion and adhesives. New York: Wiley, 1954:130–138.
[5] Kaelble DH. J Adhesion 1969;1:102.
[6] Gent AN, Petrich RP. Proc R Soc A 1969;310:433.
[7] Schupp DA, Gerberich WW. J Adhesion 1991;35:269.
[8] Mostovoy S, Ripling EJ. J Appl Polym Sci 1971;15:661.
[9] Bascom WD, Cottington RL, Jones RL, Peyser P. J Appl Polym Sci 1975;19:2545.
[10] Kinloch AJ, Shaw SJ. J Adhesion 1981;12:59.
[11] Robertson RE. J Adhesion 1972;4:1.
[12] Murray J, Hull D. J Polym Sci 1970;A-2(8):1521.
[13] Kramer EJ, Berger LL. In: Kausch HH, editor, Advances in polymer science 91/92. Berlin: Springer, 1990:1–68.
[14] Wool RP. Polymer interfaces, chapter 11. Munich: Hanser, 1995.
[15] Mendelson RA. In: Provder T, editor, Detection and data analysis in size exclusion chromatography. Washington: ACS, 1987:263–280.
[16] Shin E, Hiltner A, Baer E. J Appl Polym Sci 1992;46:213.
[17] Hsieh AJ, Schneider NS, Mandell JF. Polym Composites 1990;11:240.
[18] Nazarenko S, Hiltner A, Baer E. Unpublished results.
[19] Matsushige K, Baer E, Radcliffe SV. J Macromol Sci-Phys 1975;B11:565.
[20] Crocombe AD, Adams RD. J Adhesion 1982;13:241.
[21] Niesiolowski F, Aubrey DW. J Adhesion 1981;13:87.
[22] Wang SS, Mandell JF, McGarry FJ. Int J Fracture 1978;14:39.
[23] Michler GH. J Mater Sci 1990;25:2321.
[24] Berger LL, Kramer EJ. J Mater Sci 1987;22:2739.